
Retrieve-then-Steer: Online Success Memory for Test-Time Adaptation of Generative VLAs

Jianchao Zhao^{1,2}, Huoren Yang^{1,2}, Yusong Hu², Yuyang Gao², Qiguan Ou²,
Cong Wan¹, SongLin Dong³, Zhiheng Ma³, Yihong Gong^{1,3},

¹College of Artificial Intelligence, Xi'an Jiaotong University

²One Robotics

³Shenzhen University of Advanced Technology

Abstract

Vision-Language-Action (VLA) models show strong potential for general-purpose robotic manipulation, yet their closed-loop reliability often degrades under local deployment conditions. Existing evaluations typically treat test episodes as independent zero-shot trials. However, real robots often operate repeatedly in the same or slowly changing environments, where successful executions provide environment-verified evidence of reliable behavior patterns. We study this persistent-deployment setting, asking whether a partially competent frozen VLA can improve its reliability by reusing its successful test-time experience. We propose an online success-memory guided test-time adaptation framework for generative VLAs. During deployment, the robot stores progress-calibrated successful observation-action segments in a long-term memory. At inference, it retrieves state-relevant action chunks, filters inconsistent candidates via trajectory-level consistency, and aggregates them into an elite action prior. To incorporate this prior into action generation, we introduce confidence-adaptive prior guidance, which injects the elite prior into an intermediate state of the flow-matching action sampler and adjusts the guidance strength based on retrieval confidence. This design allows the frozen VLA to exploit environment-specific successful experience while preserving observation-conditioned generative refinement. This retrieve-then-steer mechanism enables lightweight, non-parametric test-time adaptation without requiring parameter updates. Simulation and real-world experiments show improved task success and closed-loop stability, especially in long-horizon and multi-stage tasks.

1 Introduction

Vision-Language-Action (VLA) models [2, 32, 12, 1], particularly generative VLAs [4, 9, 14] that incorporate diffusion or flow-matching mechanisms, show immense potential for general-purpose robotic manipulation by generating expressive and temporally coherent action chunks. However, a significant disconnect exists between current evaluation paradigms and real-world deployment. Most benchmarks treat testing as independent zero-shot trials, overlooking that real robots typically perform repetitive tasks in static or slowly changing environments. In such settings, physical layouts, camera viewpoints, calibration errors, and task patterns exhibit strong inter-episode correlation. Consequently, deployment should not be viewed as a series of isolated test episodes, but rather as a persistent online process operating under correlated local conditions.

Embracing this "persistent online" perspective is vital. While many existing VLAs possess strong foundational capabilities, their closed-loop execution often remains unstable during real-world deployment. Although a robot might occasionally complete a task, it is highly prone to failure in nearly identical states due to perception noise, viewpoint shifts, or accumulated errors [7, 21].

This fragility underscores the value of successful experiences. A successful grasp or placement, for instance, implicitly captures the visual geometry, actuation biases, and execution timing specific to that environment. Consequently, these trajectories should not be treated as isolated samples discarded after evaluation, but rather as environment-verified evidence that dictates reliable behavior patterns under the current physical and visual settings. This motivates our central question: *can a frozen base VLA improve its reliability by reusing its own successful test-time interactions?*

A review of existing research, however, reveals that current paradigms have yet to provide a satisfactory answer to this question. First, pre-training and downstream fine-tuning [19, 12, 9] enhance policies before deployment but fail to enable continuous learning from test-time successes. To this end, reinforcement learning and human-in-the-loop methods [11, 22] utilize deployment experience but typically require extra feedback, safe exploration, and heavy parameter updates. In contrast, recent test-time steering [27, 13, 10, 5] focuses on inference by sampling and filtering action candidates. However, these training-free approaches generally follow a myopic "generate-then-select" paradigm, discarding candidates after local evaluation. Consequently, they struggle to exploit successful experiences accumulated across repeated episodes.

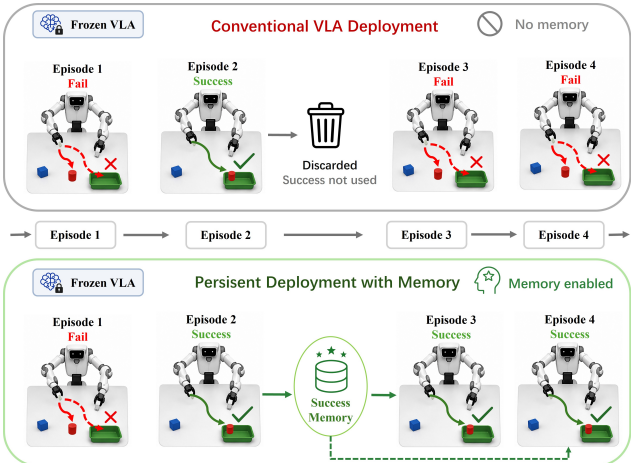


Figure 1: Motivation for persistent VLA deployment. Our method stores successful trials in online memory and reuses them to stabilize later executions without updating the policy.

Therefore, we propose directly formulating successful test-time experience as a soft behavioral prior for generative VLAs. Rather than assuming independent test episodes, we organize successful executions as reusable local evidence for future action generation. This yields a novel "retrieve-then-steer" paradigm: an online success memory compels the frozen VLA toward behavior patterns proven effective in the target environment, while preserving its ability to condition on real-time observations.

To operationalize this paradigm, we introduce an online success-memory guided test-time adaptation framework for generative VLAs. Specifically, during continuous deployment, the robot stores progress-calibrated successful observation-action prefixes while excluding failed or redundant motions. At inference, it retrieves observation-relevant action chunks, eliminates conflicting trajectories via consistency filtering, and aggregates high-quality candidates into an elite action prior. To integrate this prior into action generation, we propose confidence-adaptive prior guidance. By injecting the elite prior directly into the intermediate state of the generative sampler, the system dynamically adjusts guidance strength based on retrieval confidence. This ensures high-confidence retrievals dictate successful behavior patterns, while uncertain retrievals safely revert to the original VLA sampler.

We evaluate the proposed framework in both **simulation and real-world** robotic manipulation. Our method improves generative VLA policies on long-horizon language-conditioned manipulation benchmarks, including LIBERO-10 and SimplerEnv, and further shows consistent gains on real-world bimanual manipulation tasks. Across these settings, online success-memory guidance improves task success and closed-loop stability, especially on long-horizon and multi-stage tasks. Our contributions are threefold:

- We redefine VLA deployment as a persistent online adaptation process rather than isolated trials, highlighting successful test-time interactions as a critical source of environment-specific evidence for enhancing policy reliability.
- We propose a non-parametric "retrieve-then-steer" mechanism that enables lightweight TTA for frozen VLAs. This mechanism utilizes a progress-calibrated success memory to extract reusable segments and injects consistency-filtered elite priors into the generative sampling process, guiding the model without requiring parameter updates.

- We systematically validate the framework across long-horizon benchmarks and real-world bimanual manipulation. Results demonstrate our method significantly improves success rates and strengthens closed-loop stability in complex, multi-stage tasks.

2 Related Works

Vision-Language-Action Models. Vision-Language-Action models (VLAs) [2, 32, 12, 19, 8] have become a promising paradigm for general-purpose robotic policies by unifying visual perception, language understanding, and action generation. Early systems such as RT-1 [2] and OpenVLA [12] learn end-to-end policies from large-scale robotic data, while recent generative policies, including Diffusion Policy [4] and $\pi_0/\pi_{0.5}$ [1, 9], model continuous action chunks with diffusion or flow-matching heads. Despite these advances, VLAs still suffer from sampling noise, distribution shifts, and accumulated closed-loop errors during deployment, limiting their stability and local adaptability.

Test-Time Policy Steering. Recent work has explored test-time policy steering or scaling to improve VLA deployment stability [10, 5, 13, 27]. These methods enhance current action decisions through additional sampling, external evaluators, or internal confidence signals. For example, RoboMonkey [13] selects among perturbed action candidates with a VLM-based verifier, MG-Select [10] uses condition-masking confidence for verifier-free selection, and TACO [27] constrains generation toward stable successful modes via pseudo-count estimation. While effective, these methods follow a generate-then-select paradigm, which incurs extra inference overhead and discards reusable cross-episode experience. By contrast, our method performs prior-guided generation, retrieving successful action segments to steer the generative sampler before actions are produced.

Retrieval-Augmented and Memory-Based Robot Learning. Retrieval-augmented and memory-based mechanisms [23, 17, 18] have long been used in robot learning to improve the utilization of historical experience, demonstrations, and task context. Existing methods typically retrieve relevant trajectories from offline demonstration datasets for few-shot imitation, skill retrieval, or local policy adaptation [17, 31, 24], while others treat memory as a replay buffer for continual learning or reinforcement learning [26, 3]. Although effective, these methods often rely on offline data, use retrieval mainly as context, or require policy updates, limiting their suitability for lightweight test-time adaptation of frozen VLAs. Unlike these approaches, our method constructs memory directly during deployment from verified successful executions and uses it as a lightweight non-parametric prior for frozen VLAs, without offline demonstration banks or parameter updates.

3 Preliminaries

3.1 Problem Formulation

We consider language-conditioned robotic manipulation in downstream deployment. Let π_{vla} be a generative Vision-Language-Action policy fine-tuned on downstream demonstrations. At decision step t , given observation $o_t = (I_t^{1:N_c}, q_t)$ and instruction l , the policy samples an action chunk $a_t \sim \pi_{\text{vla}}(\cdot | o_t, l)$ with horizon H , where $I_t^{1:N_c}$ denotes multi-view RGB images and q_t denotes the proprioceptive state. During each test episode, the robot executes action chunks in closed loop, producing a trajectory $\tau^{(i)} = \{(o_t^{(i)}, a_t^{(i)})\}_{t=0}^{T_i-1}$. Unlike standard zero-shot evaluation that treats episodes independently, we study continuous deployment, where successful cross-episode experience can be accumulated and reused for test-time adaptation.

4 Methodology

4.1 Online Progress-Calibrated Memory

Since the frozen VLA cannot update its parameters during deployment, we construct an Online Progress-Calibrated Memory \mathcal{M} to store successful observation-action segments.

Trajectory buffering and memory representation. For the i -th test episode, we maintain a temporary buffer $\mathcal{B}^{(i)} = \{(k_t^{(i)}, a_t^{(i)})\}_{t=0}^{T_i-1}$ to record candidate memory entries generated during

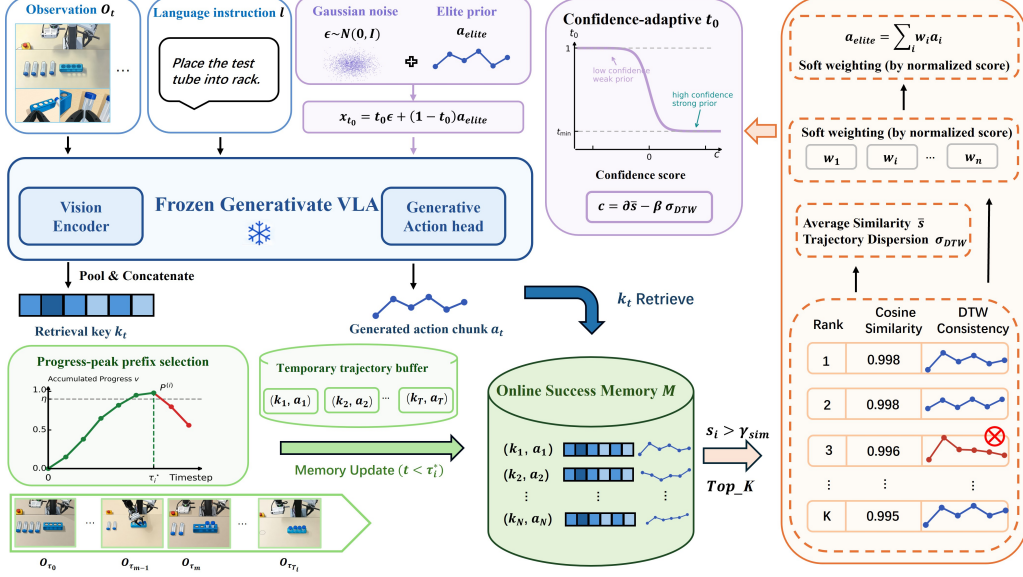


Figure 2: Overview of our retrieve-then-steer test-time adaptation framework. The frozen VLA accumulates progress-verified successful observation–action segments in an online success memory. For each new observation, relevant action chunks are retrieved, filtered, and aggregated into an elite prior, which initializes the flow-matching sampler with confidence-adaptive guidance.

execution. Here, $k_t^{(i)}$ denotes the retrieval key at time step t . Instead of introducing a separate retrieval encoder, we reuse the VLA visual encoder to extract image features. For each view, spatial patch tokens are reshaped into a feature grid, downsampled by 2×2 average pooling, and flattened. For multi-view observations, features from all views are concatenated and normalized to form $k_t^{(i)}$.

Interval-based progress calibration. To identify reusable successful experience, we instantiate the progress estimator Φ_ψ with a pretrained VLAC critic [28], which automatically evaluates trajectories for memory construction without human success labels. For each task, one successful demonstration video from the training set is used as the reference process R , serving as an in-context example of the task execution procedure. Details are provided in Appendix A.

Let Δ denote the evaluation interval. For trajectory i , we evaluate progress at timesteps $\mathcal{T}_i^\Delta = \{0, \Delta, 2\Delta, \dots, \lfloor T_i/\Delta \rfloor \Delta\} \cup \{T_i\}$. For adjacent timesteps $\tau_{m-1}, \tau_m \in \mathcal{T}_i^\Delta$, the pretrained critic predicts the signed progress change conditioned on the instruction and reference process:

$$c_{\tau_m}^{(i)} = \Phi_\psi \left(o_{\tau_{m-1}}^{(i)}, o_{\tau_m}^{(i)}, l^{(i)}; R \right), \quad (1)$$

the value of $c_{\tau_m}^{(i)}$ indicates whether the task progresses or regresses within the interval. We then accumulate interval-level progress into a trajectory-level progress score $v_{\tau_m}^{(i)}$, initialized as $v_{\tau_0}^{(i)} = 0$:

$$v_{\tau_m}^{(i)} = v_{\tau_{m-1}}^{(i)} + \left(100 - v_{\tau_{m-1}}^{(i)} \right) \frac{c_{\tau_m}^{(i)}}{100}. \quad (2)$$

Progress-peak prefix selection and memory update. After the episode finishes, we define the completion score as the maximum accumulated progress, $P^{(i)} = \max_{\tau_m \in \mathcal{T}_i^\Delta} v_{\tau_m}^{(i)}$, and denote the progress-peak timestep as $\tau_i^* = \arg \max_{\tau_m \in \mathcal{T}_i^\Delta} v_{\tau_m}^{(i)}$. We use the maximum accumulated progress instead of terminal progress to handle possible regressions after near-success, such as overshooting, collisions, or unnecessary motions. This allows the progress peak to preserve the best achieved task state and retain reusable successful experience. Given a success threshold η , the episode-level success indicator is defined as $y^{(i)} = \mathbb{I}[P^{(i)} \geq \eta]$. If $y^{(i)} = 0$, the temporary buffer is discarded; otherwise, we retain only candidate entries before the progress peak: $\mathcal{B}_+^{(i)} = \{(k_t^{(i)}, a_t^{(i)}) \in \mathcal{B}^{(i)} \mid t \leq \tau_i^*\}$. Then the online success memory is updated as $\mathcal{M} \leftarrow \mathcal{M} \cup \mathcal{B}_+^{(i)}$.

4.2 Retrieval-based Action Prior

When the online success memory \mathcal{M} is non-empty, we retrieve historical successful actions that are similar to the current state during test time, which are used to assist subsequent action generation.

Successful action retrieval with similarity gating. Given the current retrieval key k_t , for each memory entry $(k_i, a_i) \in \mathcal{M}$, we compute its relevance to the current state using cosine similarity, $s_i = \frac{\langle k_t, k_i \rangle}{\|k_t\|_2 \|k_i\|_2}$. We then select the top- K candidates with the highest similarity scores and remove weakly related results using a threshold γ_{sim} , yielding the initial candidate set \mathcal{I}_{sim} .

DTW-based trajectory consistency filtering. State-level similarity alone may still introduce action-level mismatches, where retrieved states are close to the current state but their action chunks follow inconsistent trajectory patterns. To remove such outliers, we compute pairwise multivariate Dynamic Time Warping (DTW) distances among the candidates in \mathcal{I}_{sim} :

$$d_{ij} = \text{DTW}(a_i, a_j), \quad i, j \in \mathcal{I}_{\text{sim}}. \quad (3)$$

For each candidate action chunk a_i , we define its trajectory inconsistency score as the median distance to the remaining candidates, $r_i = \text{median}_{j \in \mathcal{I}_{\text{sim}}, j \neq i} d_{ij}$. A larger r_i indicates that the candidate deviates from the dominant successful trajectory pattern. We therefore remove candidates with excessively large inconsistency scores and obtain the final candidate set \mathcal{I} .

Elite action prior aggregation. Given the filtered candidate set \mathcal{I} , we aggregate multiple successful action chunks with similarity-based soft weights, rather than directly selecting a single nearest-neighbor action. The weight of each candidate is defined as

$$w_i = \frac{\exp((s_i - \max_{j \in \mathcal{I}} s_j)/\tau)}{\sum_{j \in \mathcal{I}} \exp((s_j - \max_{m \in \mathcal{I}} s_m)/\tau)}, \quad i \in \mathcal{I}, \quad (4)$$

where $\tau > 0$ is a temperature parameter that controls the sharpness of the weight distribution. The resulting elite action prior is given by

$$a_{\text{elite}} = \sum_{i \in \mathcal{I}} w_i a_i. \quad (5)$$

This formulation provides a unified representation for action-prior aggregation. For action components in Euclidean spaces, such as positions, joint angles, we adopt linear weighted aggregation; for orientations, we compute the geodesic mean on $SO(3)$. Further details are provided in Appendix C.

4.3 Confidence-Adaptive Prior Guidance

The retrieved elite action prior a_{elite} provides a local successful behavior reference from the online success memory. However, unreliable retrievals caused by representation bias, nearest-neighbor mismatch, or trajectory inconsistency may introduce incorrect constraints. We therefore propose *confidence-adaptive prior guidance*, which injects the retrieved prior into the flow-matching sampler as a soft generative constraint and adapts its strength according to retrieval confidence.

For a VLA with a flow-matching action head, the original sampler starts from Gaussian noise $x_1 = \epsilon$, $\epsilon \sim \mathcal{N}(0, I)$ and integrates the conditional velocity field $v_\theta(x_t, t, z_t)$ from $t = 1$ to $t = 0$, where z_t is the conditioning feature from the current observation and instruction. Instead of modifying the model or velocity field, we initialize the sampling process from an intermediate state:

$$x_{t_0} = (1 - t_0)a_{\text{elite}} + t_0\epsilon, \quad \epsilon \sim \mathcal{N}(0, I). \quad (6)$$

Here, $t_0 \in [0, 1]$ controls the guidance strength. A smaller t_0 places the initial state closer to a_{elite} , yielding stronger prior guidance, while a larger t_0 preserves more randomness and recovers the original sampler.

To adapt the guidance strength to retrieval reliability, we estimate a confidence score from both state-level similarity and action-level consistency. Given the filtered candidate set \mathcal{I} , we compute the average retrieval similarity $\bar{s}_{\text{top-}K} = \frac{1}{|\mathcal{I}|} \sum_{i \in \mathcal{I}} s_i$. Since deployment similarities often lie in a narrow high-score range, we normalize it as

$$\tilde{s} = \text{clip} \left(\frac{\bar{s}_{\text{top-}K} - s_{\text{ref}}}{s_{\text{scale}}}, -c_{\text{max}}, c_{\text{max}} \right). \quad (7)$$

Table 1: Success rates (%) on LIBERO-10. Each task is evaluated over 50 trials. * denotes reproduced results. For reproduced results, the average row reports mean \pm std over three random seeds.

Task	OpenVLA [12]	π_0 -FAST [20]	π_0^* [1]	π_0 + TACO* [27]	π_0 + Ours	$\pi_{0.5}^*$ [9]	$\pi_{0.5}$ + Ours
Soup and Sauce in Basket	60.0	74.0	78.0	82.0	84.0	90.0	100.0
Cheese and Butter in Basket	76.0	72.0	98.0	94.0	92.0	100.0	100.0
Turn on Stove and Place Moka	58.0	62.0	84.0	92.0	96.0	96.0	98.0
Black Bowl in Drawer	36.0	52.0	90.0	92.0	96.0	94.0	100.0
Mugs on Plates	32.0	54.0	84.0	82.0	82.0	96.0	96.0
Book in Caddy	82.0	82.0	96.0	94.0	96.0	100.0	92.0
Mug and Pudding on Plate	60.0	58.0	82.0	82.0	80.0	94.0	94.0
Soup and Cheese in Basket	70.0	72.0	98.0	96.0	94.0	96.0	100.0
Moka Pots on Stove	20.0	26.0	30.0	36.0	38.0	64.0	70.0
Mug in Microwave	46.0	50.0	76.0	88.0	86.0	94.0	94.0
Average	54.0	60.2	81.6	83.8 (\uparrow 2.2)	84.4 (\uparrow 2.8)	92.4	94.4 (\uparrow 2.0)
	-	-	\pm 0.8	\pm 0.2	\pm 0.4	\pm 0.2	\pm 0.3

We further measure action-level dispersion using the DTW inconsistency scores, $\sigma_{\text{DTW}} = \text{Std}(\{r_i\}_{i \in \mathcal{I}})$, and define the retrieval confidence as

$$c = \alpha \tilde{s} - \beta \sigma_{\text{DTW}}, \quad (8)$$

where larger c indicates a more reliable prior. Finally, we map the retrieval confidence to the sampling starting time:

$$t_0 = t_{\min} + (1 - t_{\min})\sigma(-\gamma c), \quad (9)$$

where t_{\min} is the strongest-guidance starting time and γ controls the mapping sharpness. Higher confidence moves t_0 toward t_{\min} , while lower confidence moves it toward 1, recovering the original sampler.

After determining t_0 , the sampler starts from x_{t_0} and integrates the same conditional velocity field to $t = 0$. With Euler discretization, the update is

$$x_{t-\Delta t} = x_t - \Delta t \cdot v_{\theta}(x_t, t, z_t), \quad t : t_0 \rightarrow 0. \quad (10)$$

The final state x_0 serves as the generated action chunk $\hat{a}_{t:t+H-1}$. If the memory is empty or retrieval fails the similarity and trajectory-consistency filters, no prior is injected and the method falls back to the original sampling process. We also provide the diffusion counterpart in Appendix B.

5 Experiments

5.1 Simulation Experiments

5.1.1 Setup and Baselines

Benchmarks. We evaluate our method on two simulation benchmarks, LIBERO[16] and SimplerEnv[15]. LIBERO is a benchmark for lifelong learning in decision making, consisting of multiple task suites. As easier suites are near-saturated, we focus on the more challenging LIBERO-10 suite to examine whether our method can mitigate state drift, accumulated action errors, and unstable closed-loop execution in long-horizon, multi-stage manipulation tasks. SimplerEnv is a real-to-sim manipulation benchmark built upon the SAPIEN simulator and the ManiSkill2 benchmark, providing simulated task environments for both the WidowX and Google Robot platforms. In this work, we primarily use the tasks designed for the Google Robot platform to evaluate robustness under realistic deployment conditions, including object layout variations, visual perturbations, and fine-grained manipulation.

Baselines. We mainly evaluate our framework on VLA policies with flow-matching or diffusion-based action heads. Specifically, we select π_0 [1] and $\pi_{0.5}$ [9] as the primary baseline models for LIBERO, and adopt CogACT[14] for experiments on SimplerEnv. We also compare with TACO [27], a test-time scaling method, to evaluate our method against existing test-time steering approaches. For a more comprehensive comparison, we further report the success rates of representative VLA policies on selected benchmarks, including OpenVLA[12], π_0 -FAST [20], RT-1[2], RT-1-X[19], RT-2-X[19], and Octo[25].

Table 2: Success rates (%) on the SIMPLER benchmark. We compare our method on top of CogACT with prior VLA policies. For CogACT and CogACT + Ours, we report mean \pm std over three random seeds.

Method	Pick Coke Can	Move Near	Open/Close Drawer	Open Top Drawer and Place Apple	Average
RT-1 [2]	85.7	44.2	73.0	6.5	52.4
RT-1-X [19]	56.7	31.7	59.7	21.3	42.4
RT-2-X [19]	78.7	77.9	25.0	3.7	46.3
Octo-Base [25]	17.0	4.2	22.7	0.0	11.0
OpenVLA [12]	18.0	56.3	63.0	0.0	34.3
CogACT [14]	91.3 \pm 0.3	83.3 \pm 0.6	71.8 \pm 0.2	56.8 \pm 0.1	75.8 \pm 0.3
CogACT + Ours	94.6 \pm 0.2 (\uparrow 3.3)	85.8 \pm 0.2 (\uparrow 2.5)	75.4 \pm 0.3 (\uparrow 3.6)	62.3 \pm 0.2 (\uparrow 5.5)	79.5 \pm 0.2 (\uparrow 3.7)

Table 3: Performance comparison on the real-robot test tube placement task. The task is to pick up the test tubes one by one from left to right and place them onto the test tube rack.

Method	Success Rate (%)				Avg. Len
	1/4	2/4	3/4	4/4	
π_0 [1]	64.0	26.0	14.0	8.0	1.12
$\pi_{0.5}$ [9]	80.0	32.0	24.0	18.0	1.54
$\pi_{0.5}$ + Ours	90.0	48.0	32.0	24.0	1.94

5.1.2 Results

The simulation results are reported in Tables 1 and 2. On LIBERO-10, our method improves both base policies. For π_0 , the average success rate increases from 81.6% to 84.4%, outperforming the test-time scaling method TACO, which achieves 83.8%. For the stronger $\pi_{0.5}$ policy, our method further improves the average success rate from 92.4% to 94.4%. Task-level gains are especially clear on long-horizon and multi-stage tasks such as Turn on Stove and Place Moka, Black Bowl in Drawer, Moka Pots on Stove, and Soup and Sauce in Basket. These results show that online success memory provides reusable environment-specific action priors that help stabilize closed-loop execution.

On SimplerEnv, our method also improves CogACT from 75.8% to 79.5% on average, with consistent gains across all four tasks. The improvements are 3.3, 2.5, 3.6, and 5.5 points on Pick Coke Can, Move Near, Open/Close Drawer, and Open Top Drawer and Place Apple, respectively. The largest gain appears on the most challenging long-horizon task, suggesting that our retrieval-guided prior is effective under layout variations and visual perturbations.

5.2 Real-World Experiments

5.2.1 Setup

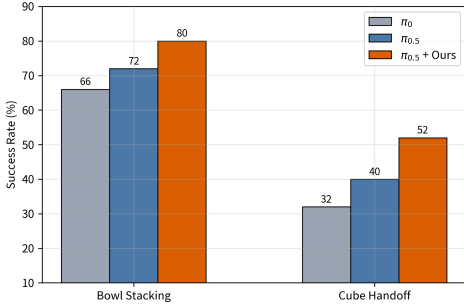
We evaluate our method on two real-world bimanual platforms: an OpenArm-based dual-arm system [6] and an ALOHA-PiPER system [29, 30]. We collect 100 training trajectories per task and evaluate four tasks: bowl stacking, cube handoff, and sequential test-tube placement on OpenArm, and bimanual T-shirt folding on ALOHA-PiPER. The tasks cover long-horizon manipulation, bimanual coordination, fine-grained placement, deformable-object manipulation, and appearance shifts. Hardware details, task definitions, and training/testing protocols are provided in Appendix D.

5.2.2 Results

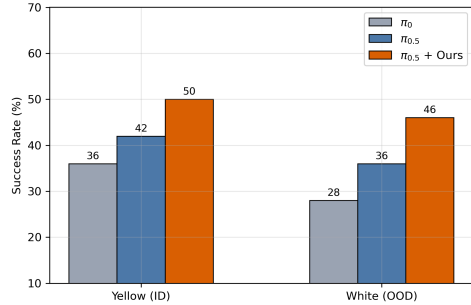
OpenArm results. The OpenArm results are reported in Figure 3(a) and Table 3. As shown in Figure 3(a), $\pi_{0.5}$ + Ours improves the success rate from 72.0% to 80.0% on Bowl Stacking and from 40.0% to 52.0% on Cube Handoff. For Sequential Test-Tube Placement, Table 3 shows that our method improves all completion stages, increasing the full 4/4 success rate from 18.0% to 24.0% and the average completed length from 1.54 to 1.94. These results indicate that online success memory improves execution stability in long-horizon and bimanual manipulation tasks.

Table 4: Component ablation on LIBERO-10. We report the average success rate (%) over all tasks. The ablation separately studies how the retrieved prior is constructed and how it is used for action generation. All intermediate-initialization variants use dynamic t_0 .

Variant	Retrieved Prior	Prior Usage	Avg. Success
Base $\pi_{0.5}$	–	Original sampler	92.4
<i>Prior-construction ablation</i>			
Top-1 Retrieval	Nearest success chunk	Intermediate init.	93.6
Top- K Soft Aggregation	Top- K weighted prior	Intermediate init.	94.0
<i>Prior-usage ablation</i>			
Direct Replay	Top- K + DTW prior	Direct execution	87.8
Output Interpolation	Top- K + DTW prior	Post-hoc interpolation	93.0
Full Ours	Top- K + DTW prior	Intermediate init.	94.4



(a) OpenArm tasks.



(b) ALOHA-PiPER cloth folding.

Figure 3: Success rates on real-world robot tasks. (a) OpenArm results on Bowl Stacking and Cube Handoff. (b) ALOHA-PiPER results on bimanual T-shirt Folding.

ALOHA-PiPER results. The ALOHA-PiPER T-shirt folding results are shown in Figure 3(b). On in-domain yellow T-shirts, $\pi_{0.5} + \text{Ours}$ improves the success rate from 42.0% to 50.0%. Under out-of-domain white T-shirts, our method improves the success rate from 36.0% to 46.0%. Averaged across both settings, it increases performance from 39.0% to 48.0%, indicating improved robustness to appearance shifts in deformable-object manipulation.

6 Ablation Studies and Analyses

Continuous deployment analysis.

Continuous deployment analysis. We evaluate continuous deployment on the *Moka Pots on Stove* task from LIBERO-10. Starting from an empty memory, the policy is tested for 300 trajectories across different random seeds. During this process, verified successful observation–action segments are progressively written into the online memory and retrieved in later episodes to guide the frozen VLA. We use a bounded memory of 3.5k entries with FIFO replacement once the capacity is reached. As shown in Figure 4(a), the cumulative success rate of the original $\pi_{0.5}$ remains stable, while $\pi_{0.5} + \text{Ours}$ gradually improves as the memory accumulates reusable experience and then stabilizes at a higher level. Notably, the gain is maintained after the memory saturates, showing that our method can exploit recent and relevant successful experience under a finite memory budget. A detailed memory-capacity ablation is provided in Appendix E.

Component ablation. We conduct component ablations on LIBERO-10 using $\pi_{0.5}$ as the frozen base policy. As shown in Table 4, Top-1 Retrieval improves the average success rate from 92.4% to 93.6%, showing that a retrieved successful chunk already provides useful test-time guidance. Top- K Soft Aggregation further increases the success rate to 94.0%, and the full method reaches 94.4%, indicating that multi-candidate aggregation and DTW-based filtering improve the retrieved prior. We

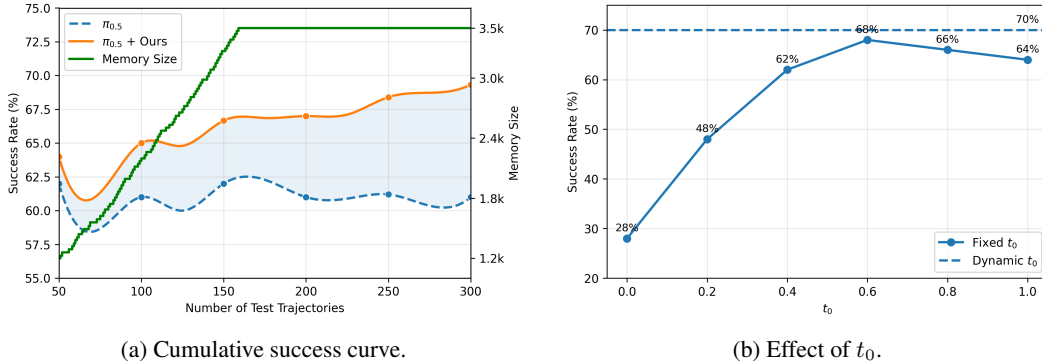


Figure 4: Analysis of continuous deployment and confidence-adaptive prior guidance.

Table 5: Ablation of success-memory construction on LIBERO-10 and evaluation of the success discriminator.

Success-Memory Construction			
Memory Type	Label Source	Progress-Peak Truncation	Avg. Success
No Memory	–	–	92.4
Unverified Memory	None	×	87.6
Oracle Successful Full Trajectory	Environment Label	✓	94.8
Predicted Successful Full Trajectory	Discriminator	×	91.8
Predicted Successful Prefix Memory	Discriminator	✓	94.4
Success Discriminator Evaluation			
Metric	Value	Metric	Value
Accuracy	0.676	Precision	0.970
Recall	0.678	F1-score	0.798

also compare different prior-usage strategies with the same Top- K + DTW prior. Direct Replay drops performance to 87.8%, suggesting that retrieved actions should not be directly executed. Output Interpolation improves over the base policy to 93.0%, but remains below intermediate initialization. These results show that injecting the prior into the generative sampler is more effective than post-hoc action reuse, as it allows the frozen VLA to refine actions under the current observation.

Effect of t_0 . We analyze the effect of t_0 on prior-guidance strength using the Moka Pots on Stove task. Fixed t_0 shows clear sensitivity: a large t_0 underuses the retrieved prior, while a small t_0 over-constrains generation and weakens observation-conditioned refinement. The best fixed setting achieves a success rate of 0.68 at $t_0 = 0.6$, whereas dynamic t_0 further improves it to 0.70, showing the advantage of confidence-adaptive guidance over manual tuning.

Effect of success-memory construction. Table 5 shows that memory quality is critical. Storing all trajectories without verification reduces the average success rate from 92.4% to 87.6%, indicating that noisy test-time experience can introduce harmful priors. Using predicted successful full trajectories also underperforms the base policy, suggesting that untrimmed trajectories may contain redundant or regressive segments. In contrast, our predicted successful prefix memory achieves 94.4%, close to the oracle memory result of 94.8%. These results confirm the importance of both reliable success verification and progress-peak truncation. Although the discriminator has moderate recall, its high precision of 0.970 is more desirable for memory construction, since a smaller but cleaner memory is preferable to one contaminated by false successful segments.

7 Conclusion

We propose an online success-memory guided test-time adaptation method for generative VLAs. During continuous deployment, successful observation–action segments are stored and retrieved as action priors to initialize the generative sampler. This enables a frozen VLA to reuse environment-

specific experience without parameter updates. Experiments in simulation and real-world bimanual manipulation show improved stability and success rates, especially on long-horizon tasks.

References

- [1] Kevin Black, Noah Brown, Danny Driess, Adnan Esmail, Michael Equi, Chelsea Finn, Niccolo Fusai, Lachy Groom, Karol Hausman, Brian Ichter, et al. π_0 : A vision-language-action flow model for general robot control. *arXiv preprint arXiv:2410.24164*, 2024.
- [2] Anthony Brohan, Noah Brown, Justice Carbajal, Yevgen Chebotar, Joseph Dabis, Chelsea Finn, Keerthana Gopalakrishnan, Karol Hausman, Alex Herzog, Jasmine Hsu, et al. Rt-1: Robotics transformer for real-world control at scale. *arXiv preprint arXiv:2212.06817*, 2022.
- [3] Yuhui Chen, Shuai Tian, Shugao Liu, Yingting Zhou, Haoran Li, and Dongbin Zhao. Conrft: A reinforced fine-tuning method for vla models via consistency policy. *arXiv preprint arXiv:2502.05450*, 2025.
- [4] Cheng Chi, Zhenjia Xu, Siyuan Feng, Eric Cousineau, Yilun Du, Benjamin Burchfiel, Russ Tedrake, and Shuran Song. Diffusion policy: Visuomotor policy learning via action diffusion. *The International Journal of Robotics Research*, 44(10-11):1684–1704, 2025.
- [5] Mingtong Dai, Lingbo Liu, Yongjie Bai, Yang Liu, Zhouxia Wang, Rui Su, Chunjie Chen, Liang Lin, and Xinyu Wu. Rover: Robot reward model as test-time verifier for vision-language-action model. *arXiv preprint arXiv:2510.10975*, 2025.
- [6] Enactic, Inc. Openarm: A fully open-source humanoid robot arm for physical ai research. <https://openarm.dev/>, 2025. Accessed: 2026-05-05.
- [7] Senyu Fei, Siyin Wang, Junhao Shi, Zihao Dai, Jikun Cai, Pengfang Qian, Li Ji, Xinzhe He, Shiduo Zhang, Zhaoye Fei, et al. Libero-plus: In-depth robustness analysis of vision-language-action models. *arXiv preprint arXiv:2510.13626*, 2025.
- [8] Zhi Hou, Tianyi Zhang, Yuwen Xiong, Haonan Duan, Hengjun Pu, Ronglei Tong, Chengyang Zhao, Xizhou Zhu, Yu Qiao, Jifeng Dai, et al. Dita: Scaling diffusion transformer for generalist vision-language-action policy. In *Proceedings of the IEEE/CVF International Conference on Computer Vision*, pages 7686–7697, 2025.
- [9] Physical Intelligence, Kevin Black, Noah Brown, James Darpinian, Karan Dhabalia, Danny Driess, Adnan Esmail, Michael Equi, Chelsea Finn, Niccolo Fusai, et al. $\pi_{0.5}$: a vision-language-action model with open-world generalization. *arXiv preprint arXiv:2504.16054*, 2025.
- [10] Suhyeok Jang, Dongyoung Kim, Changyeon Kim, Youngsuk Kim, and Jinwoo Shin. Verifier-free test-time sampling for vision language action models. *arXiv preprint arXiv:2510.05681*, 2025.
- [11] Michael Kelly, Chelsea Sidrane, Katherine Driggs-Campbell, and Mykel J Kochenderfer. Hg-dagger: Interactive imitation learning with human experts. In *2019 International Conference on Robotics and Automation (ICRA)*, pages 8077–8083. IEEE, 2019.
- [12] Moo Jin Kim, Karl Pertsch, Siddharth Karamcheti, Ted Xiao, Ashwin Balakrishna, Suraj Nair, Rafael Rafailov, Ethan Foster, Grace Lam, Pannag Sanketi, et al. Openvla: An open-source vision-language-action model. *arXiv preprint arXiv:2406.09246*, 2024.
- [13] Jacky Kwok, Christopher Agia, Rohan Sinha, Matt Foutter, Shulu Li, Ion Stoica, Azalia Mirhoseini, and Marco Pavone. Robomonkey: Scaling test-time sampling and verification for vision-language-action models. *arXiv preprint arXiv:2506.17811*, 2025.
- [14] Qixiu Li, Yaobo Liang, Zeyu Wang, Lin Luo, Xi Chen, Mozheng Liao, Fangyun Wei, Yu Deng, Sicheng Xu, Yizhong Zhang, et al. Cogact: A foundational vision-language-action model for synergizing cognition and action in robotic manipulation. *arXiv preprint arXiv:2411.19650*, 2024.
- [15] Xuanlin Li, Kyle Hsu, Jiayuan Gu, Karl Pertsch, Oier Mees, Homer Rich Walke, Chuyuan Fu, Ishkaa Lunawat, Isabel Sieh, Sean Kirmani, et al. Evaluating real-world robot manipulation policies in simulation. *arXiv preprint arXiv:2405.05941*, 2024.
- [16] Bo Liu, Yifeng Zhu, Chongkai Gao, Yihao Feng, Qiang Liu, Yuke Zhu, and Peter Stone. Libero: Benchmarking knowledge transfer for lifelong robot learning. *Advances in Neural Information Processing Systems*, 36:44776–44791, 2023.

- [17] Marius Memmel, Jacob Berg, Bingqing Chen, Abhishek Gupta, and Jonathan Francis. Strap: Robot sub-trajectory retrieval for augmented policy learning. *arXiv preprint arXiv:2412.15182*, 2024.
- [18] Soroush Nasiriany, Tian Gao, Ajay Mandlekar, and Yuke Zhu. Learning and retrieval from prior data for skill-based imitation learning. *arXiv preprint arXiv:2210.11435*, 2022.
- [19] Abby O’Neill, Abdul Rehman, Abhiram Maddukuri, Abhishek Gupta, Abhishek Padalkar, Abraham Lee, Acorn Pooley, Agrim Gupta, Ajay Mandlekar, Ajinkya Jain, et al. Open x-embodiment: Robotic learning datasets and rt-x models: Open x-embodiment collaboration 0. In *2024 IEEE International Conference on Robotics and Automation (ICRA)*, pages 6892–6903. IEEE, 2024.
- [20] Karl Pertsch, Kyle Stachowicz, Brian Ichter, Danny Driess, Suraj Nair, Quan Vuong, Oier Mees, Chelsea Finn, and Sergey Levine. Fast: Efficient action tokenization for vision-language-action models. *arXiv preprint arXiv:2501.09747*, 2025.
- [21] Ralf Römer, Adrian Kobras, Luca Worbis, and Angela P Schoellig. Failure prediction at runtime for generative robot policies. *arXiv preprint arXiv:2510.09459*, 2025.
- [22] Stéphane Ross, Geoffrey Gordon, and Drew Bagnell. A reduction of imitation learning and structured prediction to no-regret online learning. In *Proceedings of the fourteenth international conference on artificial intelligence and statistics*, pages 627–635. JMLR Workshop and Conference Proceedings, 2011.
- [23] Hao Shi, Bin Xie, Yingfei Liu, Lin Sun, Fengrong Liu, Tiancai Wang, Erjin Zhou, Haoqiang Fan, Xiangyu Zhang, and Gao Huang. Memoryvla: Perceptual-cognitive memory in vision-language-action models for robotic manipulation. *arXiv preprint arXiv:2508.19236*, 2025.
- [24] Shahram Najam Syed, Yatharth Ahuja, Arthur Jakobsson, and Jeff Ichnowski. Expres-vla: Specializing vision-language-action models through experience replay and retrieval. *arXiv preprint arXiv:2511.06202*, 2025.
- [25] Octo Model Team, Dibya Ghosh, Homer Walke, Karl Pertsch, Kevin Black, Oier Mees, Sudeep Dasari, Joey Hejna, Tobias Kreiman, Charles Xu, et al. Octo: An open-source generalist robot policy. *arXiv preprint arXiv:2405.12213*, 2024.
- [26] Yuxuan Wu, Guangming Wang, Zhiheng Yang, Maoqing Yao, Brian Sheil, and Hesheng Wang. Continually evolving skill knowledge in vision language action model. *arXiv preprint arXiv:2511.18085*, 2025.
- [27] Siyuan Yang, Yang Zhang, Haoran He, Ling Pan, Xiu Li, Chenjia Bai, and Xuelong Li. Steering vision-language-action models as anti-exploration: A test-time scaling approach. *arXiv preprint arXiv:2512.02834*, 2025.
- [28] Shaopeng Zhai, Qi Zhang, Tianyi Zhang, Fuxian Huang, Haoran Zhang, Ming Zhou, Shengzhe Zhang, Litao Liu, Sixu Lin, and Jiangmiao Pang. A vision-language-action-critic model for robotic real-world reinforcement learning. *arXiv preprint arXiv:2509.15937*, 2025.
- [29] Tony Z Zhao, Vikash Kumar, Sergey Levine, and Chelsea Finn. Learning fine-grained bimanual manipulation with low-cost hardware. *arXiv preprint arXiv:2304.13705*, 2023.
- [30] TZ Zhao, S Schmidgall, JW Kim, A Deguet, M Kobilarov, A Krieger, and C Finn. Aloha 2: An enhanced low-cost hardware for bimanual teleoperation. *arXiv preprint arXiv:2405.02292*, 2024.
- [31] Yichen Zhu, Zhicai Ou, Xiaofeng Mou, and Jian Tang. Retrieval-augmented embodied agents. In *Proceedings of the IEEE/CVF Conference on Computer Vision and Pattern Recognition*, pages 17985–17995, 2024.
- [32] Brianna Zitkovich, Tianhe Yu, Sichun Xu, Peng Xu, Ted Xiao, Fei Xia, Jialin Wu, Paul Wohlhart, Stefan Welker, Ayzaan Wahid, et al. Rt-2: Vision-language-action models transfer web knowledge to robotic control. In *Conference on Robot Learning*, pages 2165–2183. PMLR, 2023.

A Details of the Progress Estimator

Model overview. We use a pretrained VLAC critic [28] as the progress estimator for automatic trajectory evaluation and online success-memory construction. VLAC is a vision-language-action-critic model built upon InternVL, where action generation and process evaluation are unified in a multimodal autoregressive framework. In this work, we only use its critic capability. Given two visual observations and a language instruction, the critic predicts a signed progress change indicating whether the second observation is closer to the task goal than the first one. A positive value indicates forward task progress, a negative value indicates regression or deviation, and a value close to zero indicates little task-relevant change. Compared with single-state success classification, this pair-wise progress formulation provides a more fine-grained signal for long-horizon manipulation.

VLAC critic is trained from temporal supervision in successful task videos. Given a trajectory $O = (o_1, \dots, o_T)$ with task instruction l_{task} , two frames o_i and $o_{i+\Delta t}$ are sampled, and the progress label is constructed from their temporal offset:

$$c_{i,i+\Delta t} = \frac{\Delta t}{T - i}. \quad (11)$$

Forward pairs correspond to positive progress, while reversed pairs provide negative progress samples. The training further includes static-frame filtering, forward/backward joint sampling, task-completion prediction, and semantically mismatched samples, which improve robustness to stagnation, regression, and task-irrelevant visual changes. Since this learning process mainly depends on visual states and language goals rather than a unified action space, VLAC can be trained with heterogeneous human and robot trajectory data and generalizes across different embodiments and scenes.

Role of the reference video. VLAC supports in-context progress understanding through a reference process. For unseen tasks, scenes, or embodiments, a language instruction alone may not fully specify the task stages and completion condition. A reference process provides an execution example that reveals the expected temporal structure, key visual transitions, and task logic. Formally, VLAC estimates progress with an additional reference sequence as

$$c_{i,i+\Delta t} = \text{VLAC}(o_i, o_{i+\Delta t}; l_{\text{task}}, O_{\text{ref}}, o_0), \quad (12)$$

where O_{ref} can be a robot or human demonstration, and o_0 denotes the initial observation of the current trajectory. The reference process helps align the current execution with a successful example and enables one-shot transfer to new task instances.

In our framework, we provide one successful demonstration video for each task as the reference process R . The reference video is not used as action supervision and does not update the policy. It only serves as an in-context example for the VLAC critic. For example, in pick-and-place tasks, it implicitly specifies the stage order such as approaching, grasping, moving, and placing. This helps the critic distinguish forward progress from stagnation, regression, and failure more reliably than using the language instruction alone.

Usage in our framework. For the i -th test trajectory, we evaluate progress at a fixed interval Δ . Let τ_m and τ_{m-1} denote two adjacent evaluation timesteps. Conditioned on the instruction $l^{(i)}$ and the reference process R , the interval-level progress is computed as

$$c_{\tau_m}^{(i)} = \Phi_{\psi} \left(o_{\tau_{m-1}}^{(i)}, o_{\tau_m}^{(i)}, l^{(i)}; R \right). \quad (13)$$

These interval-level scores are accumulated into a trajectory-level progress score. Instead of using the terminal progress, we take the maximum accumulated progress as the completion score, which is more robust to overshooting, collisions, or redundant motions after near completion. If the maximum progress exceeds a threshold, the trajectory is considered to contain reusable successful experience. We then store only the observation-action prefix before the progress peak into the online memory, filtering out failure segments, regressions, and post-success redundancy.

Why VLAC critic. VLAC critic is well suited to our setting because our goal is not episode-level success labeling, but conservative extraction of reusable successful segments. The quality of online memory directly affects the reliability of the retrieved action prior. Thus, the estimator should identify task-relevant progress while avoiding the inclusion of failed or regressive segments. VLAC provides

such a task-conditioned pair-wise progress signal and can use a reference video as an in-context task prior without training a task-specific classifier.

This design is also compatible with frozen-VLA test-time adaptation. The progress estimator is pretrained and external to the base policy, requiring no policy parameter update and no assumption about the action representation of the underlying generative VLA. Our discriminator analysis further supports this choice. Although the overall accuracy and recall are moderate, the precision reaches 0.970. This means that the estimator may miss some successful trajectories, but trajectories predicted as successful are highly reliable. For success-memory construction, high precision is more important than high recall: missing a successful segment only slows memory growth, whereas storing a failed segment can contaminate memory and induce misleading action priors. Empirically, storing all trajectories without verification reduces the average success rate from 92.4% to 87.6%, while the predicted successful prefix memory achieves 94.4%, close to the oracle memory result of 94.8%. This indicates that a smaller but cleaner memory is preferable to a larger noisy memory for retrieve-then-steer test-time adaptation.

B Prior Guidance for Diffusion Action Heads

The main paper presents confidence-adaptive prior guidance using a flow-matching action head. For VLA policies equipped with diffusion-based action heads, the retrieved elite action prior a_{elite} can also be used to guide action generation. The key idea is to first perturb a_{elite} to an intermediate noise level following the diffusion forward process, and then let the original diffusion action generator perform the remaining conditional denoising steps.

B.1 Diffusion Action Generation

For diffusion-based action heads, an action chunk is modeled as a random variable generated by gradually denoising Gaussian noise. Given the conditioning feature z_t corresponding to the current observation and task instruction, standard diffusion sampling starts from

$$x_N \sim \mathcal{N}(0, I), \quad (14)$$

and iteratively applies the reverse denoising process:

$$x_{n-1} \sim p_\theta(x_{n-1} | x_n, z_t), \quad n = N, N-1, \dots, 1. \quad (15)$$

The final action chunk is obtained as

$$\hat{a}_{t:t+H-1} = x_0. \quad (16)$$

Here, N denotes the number of diffusion sampling steps, H denotes the action prediction horizon, and z_t is the conditional feature extracted by the VLA from the current observation o_t and language instruction l . Since standard diffusion sampling starts entirely from random noise, the generated action may be sensitive to noise initialization and local state deviations. To exploit environment-specific experience stored in the online success memory, we use the retrieved elite prior a_{elite} to guide the diffusion denoising process.

B.2 Prior Perturbation and Conditional Denoising

For DDPM/DDIM-style diffusion action heads, the forward noising process can be written as

$$q(x_n | x_0) = \mathcal{N}(x_n; \sqrt{\bar{\alpha}_n}x_0, (1 - \bar{\alpha}_n)I), \quad (17)$$

or equivalently,

$$x_n = \sqrt{\bar{\alpha}_n}x_0 + \sqrt{1 - \bar{\alpha}_n}\epsilon, \quad \epsilon \sim \mathcal{N}(0, I). \quad (18)$$

Here, $\bar{\alpha}_n$ denotes the cumulative signal coefficient in the diffusion noise schedule. As n increases, $\bar{\alpha}_n$ decreases and the sample moves from an action-like state toward a high-noise state.

When the retrieval module produces an elite action prior a_{elite} , we regard it as a local successful action endpoint and perturb it to an intermediate diffusion step n_0 using the original forward noising process:

$$x_{n_0} = \sqrt{\bar{\alpha}_{n_0}}a_{\text{elite}} + \sqrt{1 - \bar{\alpha}_{n_0}}\epsilon, \quad \epsilon \sim \mathcal{N}(0, I). \quad (19)$$

The intermediate step n_0 is determined by the confidence-adaptive guidance schedule introduced in the main text. Intuitively, a more reliable retrieved prior corresponds to a lower noise level and thus stronger prior guidance, whereas a less reliable prior corresponds to a higher noise level and leaves more freedom for the diffusion model.

The sampler then starts from x_{n_0} instead of x_N and performs the remaining reverse denoising steps:

$$x_{n-1} \sim p_\theta(x_{n-1} | x_n, z_t), \quad n = n_0, n_0 - 1, \dots, 1. \quad (20)$$

The final generated action chunk is

$$\hat{a}_{t:t+H-1} = x_0. \quad (21)$$

This procedure provides a diffusion-compatible form of prior guidance: a_{elite} is first mapped to an intermediate noisy state on the diffusion trajectory, and the original diffusion policy then completes conditional denoising under the current observation feature z_t . Therefore, the model does not simply replay the retrieved action; instead, it generates an action chunk near the neighborhood of historical successful behavior while remaining conditioned on the current state. If the online success memory is empty or the retrieved candidates fail the similarity and trajectory-consistency filters, the system does not construct a_{elite} and falls back to standard diffusion sampling from $x_N \sim \mathcal{N}(0, I)$.

C Component-Aware Aggregation of Action Priors

Action component decomposition. Since the action spaces of different robotic platforms may contain different types of control variables, directly applying element-wise linear averaging to the entire action vector is not always appropriate. We therefore adopt a component-aware aggregation strategy for constructing the elite action prior. For the h -th prediction step of the i -th candidate action chunk, we write

$$a_{i,h} = (\Delta p_{i,h}, \Delta r_{i,h}, g_{i,h}), \quad (22)$$

where $\Delta p_{i,h}$ denotes action components in Euclidean spaces, such as end-effector position increments or joint-angle increments; $\Delta r_{i,h}$ denotes orientation or orientation-increment components; and $g_{i,h}$ denotes the gripper command.

Aggregation of Euclidean action components. For action components that lie in Euclidean spaces, including end-effector positions, joint angles, and their corresponding increments, we directly apply similarity-weighted averaging:

$$\Delta p_{\text{elite},h} = \sum_{i \in \mathcal{I}} w_i \Delta p_{i,h}. \quad (23)$$

This operation is suitable for action dimensions with a linear structure and forms a smooth local action prior from multiple similar successful behaviors.

Aggregation of orientation components. For orientations and orientation increments, direct linear averaging may violate the geometry of the rotation space. Therefore, we first map each axis-angle orientation increment to the rotation group $SO(3)$:

$$R_{i,h} = \text{Exp}(\Delta r_{i,h}), \quad (24)$$

where $\text{Exp}(\cdot)$ denotes the exponential map from the Lie algebra $\mathfrak{so}(3)$ to $SO(3)$. We then compute the weighted geodesic mean on $SO(3)$:

$$R_{\text{elite},h} = \arg \min_{R \in SO(3)} \sum_{i \in \mathcal{I}} w_i \|\text{Log}(R_{i,h}^\top R)\|_2^2, \quad (25)$$

where $\text{Log}(\cdot)$ denotes the logarithm map from $SO(3)$ to $\mathfrak{so}(3)$. Finally, the averaged rotation is mapped back to the axis-angle representation:

$$\Delta r_{\text{elite},h} = \text{Log}(R_{\text{elite},h}). \quad (26)$$

This procedure ensures that orientation aggregation respects the geometry of the rotation manifold and avoids the inconsistency that may arise from naive linear averaging.

Aggregation of gripper actions. Since different robotic platforms parameterize gripper commands differently, we use an adaptive aggregation rule for gripper actions. For continuous gripper commands, such as gripper width, finger-joint position, or normalized continuous control values, we apply weighted averaging:

$$g_{\text{elite},h} = \sum_{i \in \mathcal{I}} w_i g_{i,h}, \quad (27)$$

and clip the result to the valid action range. For discrete gripper commands, such as open-or-close commands, we use weighted voting:

$$P_h(c) = \sum_{i \in \mathcal{I}} w_i \mathbb{I}[g_{i,h} = c], \quad (28)$$

$$g_{\text{elite},h} = \arg \max_c P_h(c). \quad (29)$$

When the retrieved gripper commands exhibit strong conflicts between opening and closing directions, we adopt a conservative fallback strategy: the gripper command from the most similar nearest-neighbor candidate is used. This avoids averaging contradictory gripper actions into an ambiguous gripper prior.

Final action prior. After component-aware aggregation, the elite action prior at the h -th prediction step is written as

$$a_{\text{elite},h} = (\Delta p_{\text{elite},h}, \Delta r_{\text{elite},h}, g_{\text{elite},h}). \quad (30)$$

By concatenating the priors over all prediction steps, we obtain the complete elite action prior:

$$a_{\text{elite}} = \{a_{\text{elite},h}\}_{h=1}^H. \quad (31)$$

This design allows our method to support end-effector pose control, joint-space control, and different gripper parameterizations, thereby avoiding overfitting the method formulation to a specific dataset or robotic platform.

D Real-World Robot Experiment Details

D.1 Hardware Platforms and Camera Configuration

We evaluate our method on two real-world bimanual robot platforms: an OpenArm-based dual-arm system and an ALOHA-PiPER system. The OpenArm platform consists of two 7-DoF humanoid robot arms equipped with parallel grippers, while the ALOHA-PiPER platform follows an ALOHA-style bimanual setup and uses two 6-DoF AgileX PiPER arms with two-finger grippers. These two platforms provide complementary testbeds for evaluating our method across different arm kinematics, gripper designs, and workspace layouts.

Both platforms take multi-view RGB images and proprioceptive states as policy inputs. Specifically, each platform is equipped with three camera views: two wrist-mounted cameras attached to the left and right grippers, and one external third-person camera. The wrist cameras provide close-up observations of local manipulation regions, such as grasping, handoff, and placement areas, while the third-person camera provides a global view of the workspace, including object layouts, arm configurations, and overall task progress.

The placement of the third-person camera differs slightly between the two platforms due to hardware constraints. On the ALOHA-PiPER platform, the external camera is mounted above the center region between the two arms on the same side as the robot arms, providing a direct overhead view of the T-shirt manipulation area. On the OpenArm platform, due to the limited mounting space on the robot side, the external camera is placed above the center region between the two arms but on the opposite side of the workspace. Although the camera placements are different, both configurations provide complementary global observations together with the two wrist-mounted views, enabling the policy to perceive both fine-grained local interactions and long-horizon task progress.

D.2 Task Definitions

We design four real-world manipulation tasks to evaluate the proposed method, covering long-horizon object manipulation, bimanual coordination, fine-grained placement, and deformable-object manipulation.

Bowl Stacking. In this task, the two robot arms grasp one bowl from each side of the workspace and stack the two bowls in the center region. The task requires the policy to coordinate both arms to complete grasping, transportation, alignment, and stacking. This task mainly evaluates long-horizon object manipulation, bimanual spatial coordination, and relative pose alignment between objects. The main challenges come from unstable bowl grasps, the need for accurate rim alignment, and the risk of collision or slippage during the stacking stage.

Cube Handoff. In this task, the right arm first picks up a red cube from a bowl on the right side of the workspace, transfers it to the left arm, and the left arm then places it into a bowl on the left side. This task evaluates bimanual handoff ability, including grasping, approaching, pose alignment between two grippers, object transfer, release timing, and final placement. Compared with single-arm pick-and-place tasks, Cube Handoff requires more precise coordination between the two end-effectors. A small error in relative gripper pose or release timing can easily cause the cube to drop.

Sequential Test-Tube Placement. In this task, the right arm sequentially picks up four test tubes arranged on the table from left to right and places them into a test-tube rack. This task evaluates long-horizon sequential manipulation, fine-grained grasping, and precise placement into narrow slots. Since test tubes are thin and elongated objects, they are difficult to grasp stably, and the rack holes impose strict requirements on placement position and orientation. To improve task success and better exploit the bimanual setup, we keep the left arm stationary during execution and orient its wrist camera toward the test-tube rack. This provides a fine-grained local view of the rack region, helping the policy observe the target holes more accurately. The main challenges include accumulated errors over repeated operations, unstable grasping of thin objects, precise insertion, and state drift during long-horizon execution.

Bimanual T-shirt Folding. On the ALOHA-PiPER platform, we evaluate a bimanual T-shirt folding task. The two arms need to collaboratively grasp key regions of the T-shirt and complete the folding process. Unlike rigid-object manipulation, T-shirt folding involves deformable-object dynamics, where the object shape changes continuously during grasping, dragging, and folding. This task therefore requires robust visual understanding and closed-loop action adjustment. Demonstrations are collected using a yellow T-shirt, while testing is conducted under both in-domain and out-of-domain settings. The in-domain setting uses yellow T-shirts, whereas the out-of-domain setting uses T-shirts with unseen colors. This design evaluates the robustness of the policy to visual appearance shifts in deformable-object manipulation. The main challenges include uncertain cloth deformation, self-occlusion, localization of key grasping regions, and visual distribution shifts caused by color changes.

D.3 Training and Testing Protocol

For each real-world task, we collect 100 demonstration trajectories to fine-tune the base VLA policy. We use the same basic training configuration across all tasks, with a batch size of 64 and a learning rate of 2.5×10^{-5} . The number of training steps is adjusted according to the task horizon and manipulation complexity, ranging from 8k to 10k steps. For relatively shorter tasks, such as Bowl Stacking and Cube Handoff, the policy is trained for around 8k steps. For longer-horizon or more fine-grained tasks, such as Sequential Test-Tube Placement and Bimanual T-shirt Folding, the number of training steps is increased toward 10k steps to better cover the full task procedure and key manipulation stages.

During evaluation, the base VLA policy is kept frozen, and no additional gradient updates or online fine-tuning are performed. Each real-world task is evaluated over 50 trials. For fair comparison, the baseline policy and our method are tested under the same set of initial states. We only enable the proposed online success-memory mechanism on top of the frozen policy. During the evaluation of each task, the online memory is initialized and continuously updated according to our success-memory construction mechanism. Specifically, the robot executes action chunks generated by the frozen VLA policy during continuous test-time deployment, and reusable observation-action segments are stored into the online success memory when successful experience is identified. In subsequent trials, the system retrieves relevant successful experience according to the current observation and uses the retrieved action prior to guide the generative action sampling process. This protocol ensures that the performance improvement comes from non-parametric test-time memory retrieval and prior-guided

Table 6: Effect of memory capacity on continuous deployment. We evaluate $\pi_{0.5}$ + Ours on the *Moka Pots on Stove* task for 300 test trajectories. C denotes the maximum number of stored observation-action entries. When the memory exceeds C , FIFO eviction is applied.

Memory Capacity C	Eviction	Final Mem. Size	Final Cum. SR (%)
0	–	0	61.0
1k	FIFO	1.0k	64.0
2k	FIFO	2.0k	66.2
3k	FIFO	3.0k	68.5
4k	FIFO	4.0k	70.2
5k	FIFO	5.0k	70.8
Unlimited	–	All	71.2

Table 7: Relative inference time normalized by the frozen base policy. “Ours w/o Retrieval” measures the prior-guided sampler after the elite prior is available, while “Ours Full” includes retrieval, filtering, prior aggregation, and action generation.

Method	Retrieval Included	Relative Time
Base VLA	–	1.00×
Ours w/o Retrieval	No	0.95×
Ours Full	Yes	1.10×

generation, rather than from additional policy training, parameter updates, or different initial-state distributions.

E Effect of Memory Capacity

As shown in Table 6, increasing the memory capacity consistently improves the final cumulative success rate, indicating that a larger memory provides more reusable successful experience for retrieval-guided action generation. The improvement is more pronounced when the capacity increases from 0 to 3k entries, while the gain gradually saturates beyond 4k. In particular, the 5k memory budget achieves a final cumulative success rate of 70.8%, which is close to the unlimited-memory setting of 71.2%. This suggests that our method does not rely on an ever-growing memory, but can achieve near-saturated performance with a bounded memory budget and FIFO replacement.

F Inference-Time Analysis

We further analyze the inference-time overhead introduced by the proposed retrieve-then-steer mechanism. All results are reported as relative inference time normalized by the frozen base policy. The runtime includes action generation for the current decision step. For our method, we report two settings: one excluding retrieval overhead, which measures only the prior-guided generative sampling process, and one including the full retrieval, filtering, aggregation, and sampling pipeline.

As shown in Table 7, the proposed method does not introduce heavy inference overhead. When the retrieval cost is excluded, our prior-guided sampler is slightly faster than the base policy, reducing the normalized inference time from 1.00× to 0.95×. This is because the retrieved elite prior initializes the generative process from an intermediate state, allowing the sampler to perform fewer effective generation steps than the original noise-starting sampler.

When retrieval, trajectory-consistency filtering, and prior aggregation are included, the full method requires 1.10× the inference time of the base policy. This moderate overhead mainly comes from nearest-neighbor search and candidate filtering in the online success memory. Since these operations are non-parametric and do not require additional forward passes through the VLA or parameter updates, the overall runtime remains lightweight. Combined with the success-rate gains reported in the main experiments, these results suggest that the proposed retrieve-then-steer mechanism offers a favorable trade-off between deployment efficiency and closed-loop reliability.

Table 8: Hyperparameter sensitivity on LIBERO-10. We report the average success rate (%) over all tasks. The default setting is highlighted in gray.

Hyperparameter	Value	Avg. Success (%)
Base $\pi_{0.5}$	–	92.4
Top- K retrieval size	$K = 1$	93.6
	$K = 3$	93.8
	$K = 5$	94.1
	$K = 10$	94.4
	$K = 20$	94.2
Similarity threshold γ_{sim}	0.9988	93.7
	0.9990	94.1
	0.9992	94.4
	0.9995	94.0
	0.9998	93.5
Aggregation temperature τ	0.01	93.8
	0.03	94.2
	0.05	94.4
	0.10	94.1
	0.20	93.9
Success threshold η	0.85	93.8
	0.90	94.1
	0.95	94.4
	0.975	94.2
	0.99	93.9

Table 9: Default hyperparameters for adaptive prior guidance. These parameters are kept fixed across experiments and are empirically stable within reasonable ranges.

Hyperparameter	Value
Reference similarity s_{ref}	γ_{sim}
Similarity scale s_{scale}	5×10^{-4}
Clipping range c_{max}	50
Similarity coefficient α	1.0
DTW-dispersion coefficient β	0.05
Mapping sharpness γ	2.0

G Hyperparameter Sensitivity

We analyze the sensitivity of the proposed retrieve-then-steer framework to key hyperparameters in the retrieval, memory construction, and prior-construction pipeline. Unless otherwise specified, experiments are conducted on LIBERO-10 using $\pi_{0.5}$ as the frozen base policy. We vary one hyperparameter at a time while keeping the others fixed to the default setting: $K = 10$, $\tau = 0.05$, $\gamma_{\text{sim}} = 0.9992$, and success threshold $\eta = 0.95$. The base policy achieves an average success rate of 92.4%.

As shown in Table 8, the proposed method is relatively robust to a broad range of hyperparameter choices. First, increasing the retrieval size from $K = 1$ to $K = 10$ consistently improves performance, indicating that aggregating multiple successful chunks provides a more reliable action prior than using a single nearest neighbor. However, further increasing K to 20 slightly reduces the success rate, likely because less relevant trajectories are introduced into the candidate set.

Second, the similarity threshold γ_{sim} controls the trade-off between prior coverage and prior quality. A lower threshold accepts more retrieved candidates but may include mismatched action chunks, while an overly strict threshold rejects useful candidates and causes the method to fall back to the base sampler more frequently. The default value $\gamma_{\text{sim}} = 0.9992$ achieves the best balance between filtering unreliable retrievals and preserving sufficient reusable experience.

Third, the aggregation temperature τ affects the sharpness of the similarity-based soft weights. A very small temperature makes the aggregation close to nearest-neighbor selection, whereas a large temperature assigns nearly uniform weights to retrieved candidates. The best performance is obtained at $\tau = 0.05$, suggesting that softly emphasizing the most relevant successful chunks while still aggregating multiple candidates yields a more stable prior.

Finally, the success threshold η controls the quality of online memory construction. A smaller threshold allows more trajectories to be written into memory, but may introduce noisy or partially failed segments. In contrast, an overly strict threshold improves memory precision but slows down memory growth and reduces retrieval coverage. The default value $\eta = 0.95$ provides a stable balance between memory quality and memory availability.

For adaptive prior guidance, we use the default configuration in Table 9. We set s_{ref} to the same value as the retrieval threshold γ_{sim} , since both measure whether a retrieved candidate is sufficiently close to the current observation. The scale $s_{\text{scale}} = 5 \times 10^{-4}$ is used to magnify small differences in high cosine-similarity regimes. The clipping range $c_{\text{max}} = 50$ prevents extreme confidence values from dominating the mapping. The coefficients $\alpha = 1.0$ and $\beta = 0.05$ balance state-level similarity and action-level dispersion, while $\gamma = 2.0$ controls the sharpness of the confidence-to-guidance mapping. We find that these parameters are not sensitive within reasonable ranges, and the default setting works consistently across tasks.

Overall, these results suggest that the performance gain does not depend on a narrowly tuned hyperparameter choice, and the default configuration provides a stable trade-off between retrieval coverage, memory quality, and action-prior robustness.

H Visualization

Additional qualitative results, including more videos and real-world robot demonstrations, are available at the following anonymous link: <https://anonymous.4open.science/r/nips2026-1D23/>

I Limitations and Future Work

Although our retrieve-then-steer framework improves the reliability of frozen generative VLAs, it still has several limitations. First, the method is designed for persistent deployment in relatively stable or slowly changing environments. Its effectiveness depends on the existence of reusable cross-episode experience; when object layouts, camera viewpoints, task goals, or robot calibration change rapidly, previously stored action priors may become less informative or even misleading. Second, the method requires the base policy to occasionally produce successful trials so that the online memory can be initialized and expanded. If the frozen VLA is far from competent on a target task, the memory may grow slowly and provide limited benefit.

Third, memory quality depends on the reliability of the progress or success estimator. Although our progress-calibrated prefix selection is designed to avoid storing failed, regressive, or post-success redundant segments, inaccurate progress estimation may still introduce noisy entries or discard useful successful experience. This issue is especially important because a small number of false successful entries can contaminate the retrieved prior and affect later generations. Fourth, retrieval based on visual similarity and trajectory consistency cannot fully resolve state aliasing. Visually similar states may require different actions due to subtle differences in object pose, contact state, occlusion, or task phase, which may lead to mismatched action priors even after similarity gating and consistency filtering.

Finally, our current memory management uses simple bounded storage and replacement strategies. While this is sufficient for the evaluated settings, larger-scale deployment may require more structured memory organization, long-term forgetting, task-aware indexing, and mechanisms for detecting environment changes. Future work will explore more reliable success verification, uncertainty-aware retrieval, scalable memory management, and adaptation to more dynamic environments with changing tasks and layouts.